Photogeneration of coherent shear phonons in orientated wurtzite semiconductors by piezoelectric coupling

Yu-Chieh Wen,[1] Tsung-Shine Ko,[2] Tien-Chang Lu,[2] Hao-Chung Kuo,[2] Jen-Inn Chyi,[3] and Chi-Kuang Sun[1,4,*]

[1]*Department of Electrical Engineering and Graduate Institute of Photonics and Optoelectronics, National Taiwan University, Taipei 10617, Taiwan*

[2]*Department of Photonics and Institute of Electro-Optical Engineering, National Chiao Tung University, Hinchu 300, Taiwan*

[3]*Department of Electrical Engineering, National Central University, Jhongli 32054, Taiwan*

[4]*Research Center for Applied Sciences, Academia Sinica, Taipei 115, Taiwan*

(Received 18 March 2009; revised manuscript received 17 September 2009; published 6 November 2009)

Using piezoelectric wurtzite semiconductor with accurate control of the crystal cut, we investigate the photogeneration of coherent shear acoustic phonons through anisotropic piezoelectric coupling. Theoretical study suggests the dominant contribution of the piezoelectric effect to the shear phonon generation in *a*-plane wurtzite GaN, which is also confirmed by the picosecond ultrasonic experiments with different dopant and excitation conditions. Piezoelectric transduction thus explains the observed remarkable coherent shear phonon signal. The influence of the ultrafast screening of surface electric field by photocarriers on the intensity and waveform of the generated shear acoustic pulse are discussed.

DOI: 10.1103/PhysRevB.80.195201 PACS number(s): 73.50.−h, 43.35.+d, 77.65.−j

When materials are shined by optical pulses, excitation of photocarriers provides an instantaneous force shaking atoms out of their equilibrium positions. Dynamics of the consequent coherent acoustic phonons reflects interatomic interactions and energy transduction with other carriers. It is thus of great interest due to the potential in exploring elastic properties and carrier-lattice interactions on the atomic-length-to-nanometer scales.[1,2] However, previous studies on coherent phonon dynamics were almost limited in the longitudinal one of three polarizations.[1,2] Difficulties in generation and detection of the other two transverse (shear) modes result that their behaviors in most matters have not been well understood while they are essential to high-frequency shear acoustic properties.[3–9]

In opaque media, shallow optical penetration depth compared with the optical spot size generally causes a high propagation directivity of the photogenerated acoustic waves (coherent acoustic phonons) along the surface normal. If the traction on the surface is laterally isotropic, atoms will not be driven along the surface so that no coherent shear phonon is excited directly through photocarriers but they can be generated by interface mode conversion.[3,10] However, with an angular-dependent conversion efficiency, it is hard to initiate high-amplitude shear modes with a planar wavefront by mode conversion. To directly activate shear modes by photocarriers, the lateral force symmetry on the surface should be broken. Anisotropic thermoelastic stress, deformation potentials, impulsive stimulated Raman scattering, and piezoelectric effect can then contribute to the generation of coherent shear phonons.[4–6] For this, surfaces with the corresponding normal not coincide with the symmetric axes of the materials are required.

For previous observations in semiconductors, the signals of coherent shear phonons are generally much weaker than that of the longitudinal mode.[4,6] This contrast suggests relatively higher longitudinal strain and/or better corresponding detection sensitivity.[11] Complex lattice deformation makes the corresponding dynamics and the associated carrier-lattice interactions complicated. To explore the concerned high-frequency shear acoustics, enhancement of the amplitude of the excited shear waves compared with the longitudinal mode is essential, which could be achieved through manipulating anisotropic carrier-phonon transductions. Among all conversion mechanisms, piezoelectric coupling was proved to provide strong driving force for initiating coherent phonons, i.e., more efficient transduction between photocarriers and acoustic waves, in semiconductors without an inversion center.[2,12,13] Assisted by this efficient channel, observations of giant coherent *longitudinal acoustic* phonon oscillations have been reported in the wurtzite InGaN/GaN quantum wells.[2]

In this paper, piezoelectric contribution to the coherent *shear* phonon generation was investigated in wurtzite semiconductors by manipulating anisotropic piezoelectric transduction with different crystal orientations. The observed optical modulation induced by shear phonons could be on the order of or higher than that by longitudinal phonons. Both theory and experiments verified the dominant contribution of piezoelectricity to the detected shear phonon signals. The effect of the screening of the surface electric field on the formation of picosecond shear acoustic pulse was also experimentally studied.

A macroscopic elastic theory was developed first to estimate the effect of crystal orientation on the excitation of different phonon modes. Photoinduced stress was introduced by considering the piezoelectric and deformation-potential couplings while the thermoelastic effect was ignored due to its minor role in semiconductors.[13,14] The electronic stress (deformation potentials) is originated from the modification of elastic force holding the ions together due to the presence of free carriers, which is proportional to the photocarrier density. On the other hand, the piezoelectric stress is coupled with the electric displacement through the lattice piezoelectric polarization, which deforms the lattices as the electric field inside samples is altered by space charges. In illuminated bulk semiconductors, surface electric field serves as an

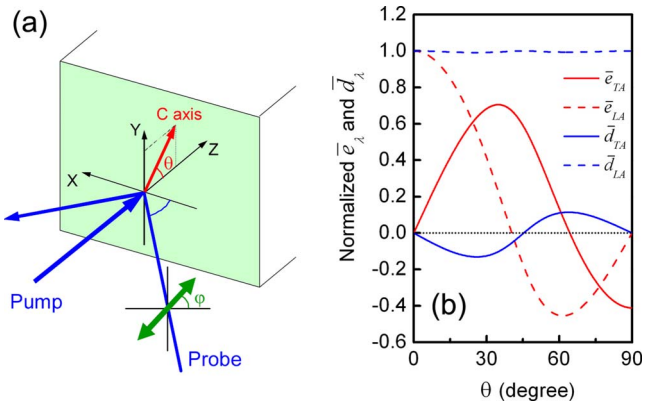

FIG. 1. (Color online) (a) Schematic diagram of experimental setup and (b) normalized $\bar{e}_\lambda$ and $\bar{d}_\lambda$, where λ=LA and TA, in wurtzite GaN as a function of crystal orientation. Two $\bar{e}_\lambda$ and two $\bar{d}_\lambda$ lines were normalized by $\bar{e}_{\mathrm{LA}}(\theta=0°)$ and $\bar{d}_{\mathrm{LA}}(\theta=0°)$, respectively. Material parameters used in the calculation were taken from Refs. 13 and 15.

environment creating space charge field and the corresponding field screening launches picosecond acoustic pulses toward the substrate by the piezoelectric effect.

By assuming relatively large illuminated areas with no built-in electric field parallel to the surface, the photocarrier distributions $[\rho_\upsilon(z,t)$, $\upsilon=e,h$ for electron and hole, respectively] and propagation of the excited acoustic waves can be reduced to be one dimensional along the surface normal [z axis in Fig. 1(a)]. For an arbitrary propagation direction, acoustic waves in anisotropic materials can be expressed as superpositions of three eigenmodes, i.e., one quasi-longitudinal-acoustic (QLA) and two quasi-transverse-acoustic (QTA) modes in general. The corresponding wave equation for each eigenmode is then derived[13] and given by

$$\frac{\partial^2 u_\lambda}{\partial t^2} - c_\lambda^2 \frac{\partial^2 u_\lambda}{\partial z^2} = \frac{1}{\rho_0}(f_{\lambda,PZ} + f_{\lambda,DP}),$$

$$\lambda = \mathrm{QLA},\ \mathrm{QTA1},\ \text{and}\ \mathrm{QTA2}, \tag{1}$$

where u_λ is the displacement along the direction of the polarization, i.e., displacement fields of the eigenmodes, c_λ is the corresponding phase velocity, and ρ_0 is the mass density. The excitation forces induced by the piezoelectric effect and the deformation potentials upon each propagation mode λ are expressed as

$$f_{\lambda,PZ} = |e|\bar{e}_\lambda[\rho_e - \rho_h]/\bar{\varepsilon}_S, \tag{2a}$$

$$f_{\lambda,DP} = \sum_{\upsilon=e,h} \bar{d}_{\upsilon\lambda}(\partial\rho_\upsilon/\partial z), \tag{2b}$$

respectively. Here $|e|$ and $\bar{\varepsilon}_S$ are the elementary charge and the static dielectric constant along the surface normal. Please note that the driving forces are proportional to the effective piezoelectric coefficient $\bar{e}_\lambda$ or the effective deformation potentials $\bar{d}_{\upsilon\lambda}$.[16] We thus can use those factors to estimate the influence of crystal orientation on the excitation of different acoustic modes.

In wurtzite crystals, one of the eigenmodes is purely transverse with polarization perpendicular to the sagittal plane [y-z plane in Fig. 1(a)]. This mode is not excited because the projection of driving forces in this direction is always zero. Figure 1(b) shows the normalized $\bar{e}_\lambda$ and $\bar{d}_\lambda$ for the other two eigenmodes in wurtzite GaN as a function of the orientation angle θ (the angle between the crystal axis and the surface normal). We can find that $\bar{d}_{\mathrm{LA}}$ is almost constant while the piezoelectric contributions strongly depend on the orientation. $\bar{e}_{\mathrm{LA}}$ has a maximum at $\theta=0°$ and two nodes at $\theta=40°$ and 90°. In addition, $\bar{e}_{\mathrm{TA}}$ has two extremes at $\theta=35°$ and 90°.

With a significant orientation dependency, this analysis suggests a possibility of creating optical-piezoelectric transducers with controllable excitations of QTA and QLA modes by manipulating crystal orientation. To demonstrate this feasibility and generate high-amplitude shear waves, we used femtosecond pump-probe technique to study photoacoustic generation in c-plane ($\theta=0°$) and a-plane ($\theta=90°$) GaN, where the concerned piezoelectricity *only* contributed to the longitudinal and shear wave generation individually. In addition, two excited acoustic modes were purely longitudinal (LA) and purely transverse (TA) with polarizations on the sagittal plane, i.e., we have two nonzero strain components $\eta_3=\eta_{zz}$ and $\eta_4=2\eta_{yz}$.

The c-(a-) plane GaN thin film was grown on c-(r-) plane sapphire by metal-organic chemical-vapor deposition. Thickness of the c-plane GaN layer was $\sim$3.5 μm.[17] Two a-plane samples with different doping conditions were investigated.[18] One was an unintentionally doped film with a 2.5 μm thickness. With intrinsic dopants, this layer exhibited n-type characteristics with a $\sim 10^{17}$ cm^{-3} doping density. The other a-plane sample has an additional p-type doped epilayer (550 nm) on the top of the unintentionally doped GaN buffer layer. The ionized hole density in this p-type layer was 5×10^{17} cm^{-3}. According to the surface electricity, the a-plane samples with (without) the p-type doped layer were referred to as the p-(n-) type sample in the following.

Optical detection of the acoustic waves in anisotropic media has been carefully analyzed in the recent reports,[5,7] which relied on the strain-induced permittivity change through three mechanisms: the local rotation, the interface interference, and the photoelastic effect. Generally speaking, the former two results in a transient change in the optical properties of media when the acoustic waves transmit/reflect at interfaces.[7] For the studied "thick" films in which buried mechanical interfaces are far from the region of optical penetration, only the latter, the photoelastic effect, contributes to the detection of the propagating coherent phonons. Qualitative analysis of the photoelastic effect is thus executed for gaining an insight into the acoustic detection in the studied case.

Although the photoelastic tensor P_{IJ} of wurtzite GaN (6 mm hexagonal symmetry) has six independent components,[19] its expression in the discussed spatial coordinates is not complicated because the crystal axis of the studied samples is either parallel or perpendicular to the surface normal. Considering the strain components η_3 and η_4, the change in the permittivity tensor $\Delta\varepsilon_I=P_{IJ}\eta_J$ for (non)orientated sample with $\theta=90°$ ($\theta=0°$) is

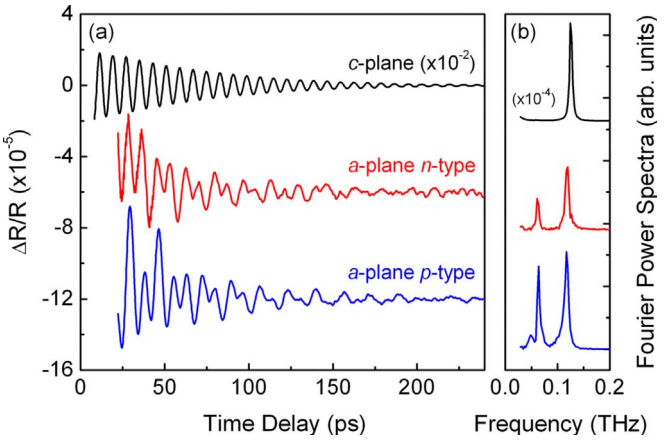

FIG. 2. (Color online) (a) Measured transient optical reflectivity and (b) the corresponding Fourier power spectra for three studied samples. The electronic backgrounds on the data were removed for clarity.

$$\Delta\varepsilon = \begin{pmatrix} P_{12}\eta_3(P_{13}\eta_3) & 0 & 0 \\ 0 & P_{31}\eta_3(P_{13}\eta_3) & P_{44}\eta_4(P_{44}\eta_4) \\ 0 & P_{44}\eta_4(P_{44}\eta_4) & P_{11}\eta_3(P_{33}\eta_3) \end{pmatrix}, \tag{3}$$

where the shear strain η_4 exists only in $\Delta\varepsilon_4$ $(=\Delta\varepsilon_{yz}=\Delta\varepsilon_{zy})$ which affects the optical reflectivity R under specific geometric condition of light incidence. To be sensitive to shear wave propagation, the optical probe was obliquely incident and chosen to be on the tangential plane (x-z plane). In this geometry, the off-diagonal term $\Delta\varepsilon_4$ scattered p-polarized incident light into s-polarized one and vice versa. Those scattered light interfered with the reflected optical probe by using a mixed probe polarization. This made reflectivity change also sensitive to the propagating shear strain.[20]

Figure 1(a) shows the schematic diagram of the experiments. The light source for the degenerate optical pump-probe setup was a frequency-doubled Ti:sapphire laser with ~200 fs pulsewidth. Central wavelength of the optical pulses was $\lambda_{op}=363$ nm, above the band gap of GaN. The optical pump was incident onto the samples normally with a pulse energy of ~0.1 nJ and a focused diameter of 20 μm. The optical probe was 45° obliquely incident with an effective spot diameter of 18 μm. With the special concern for the acoustic generation process, the probe polarization was fixed and chosen to be $\varphi=\sim 30°$ for shear wave signal optimization.

Figures 2(a) and 2(b) show the transient reflectivity changes and the corresponding power spectra for three studied samples. Electronic background on the time-domain data was removed for clarifying the acoustic signals. From the temporal traces, decaying oscillations at 125 GHz frequency was found in the c-plane sample while those in the a-plane samples had a noticeable beating between 117 and 63 GHz oscillations. Those oscillations were attributed to backward Brillouin scatterings with a frequency formulated as $f=2nV\cos\phi/\lambda_{op}$, where n is refractive index, V is sound velocity, and ϕ is the angle between the direction of light propagation inside media and the surface normal. In a-plane samples where $n=2.66$ and $V_{LA}=7833$ m/s,[15,21] the frequency of LA phonon-induced Brillouin oscillations was calculated to be 111 GHz, agreeing with the experimental observations. The sound velocity of the other low-frequency mode was estimated to be 4240 m/s according to the measured frequency. This value indicated that this mode was purely transverse and polarized along the c axis according to previous published data,[22] consistent with our theoretical prediction that the photoinduced driving forces are on the sagittal plane. On the other hand, only LA phonons were observed in the c-plane sample due to the lack of the excitation force on the shear mode.

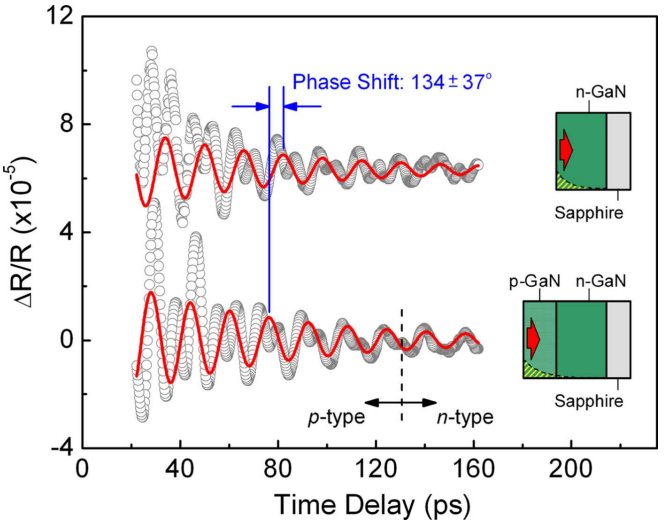

FIG. 3. (Color online) Transient optical reflectivity (circles) measured in two studied a-plane samples and the corresponding low-frequency fitting curves (solid lines). Details of data fitting are discussed in the text. The traveling time at which the shear wave propagates through the p-type layer is marked on the data. The sample structures are also shown, where arrows depict the propagation of the generated acoustic phonons and the detection region in each sample is represented by the yellow dashed area.

For the a-plane samples, optical modulation induced by the shear phonons $(\Delta R/R\sim 2\times 10^{-5})$ were manifest in comparison with the LA phonon signal. Each mode was individually fitted by a damped cosine function of the form: $A_\lambda \exp(-t/\tau_\lambda)\cos(\omega_\lambda t+\Psi_\lambda)$, where λ=TA or LA. Fitting curves for the TA-phonon signals are emphasized in Fig. 3. Here the angular frequency ω_{TA} was determined by the measured spectra and the damping time constant τ_{TA} in both samples was ~65 ps, corresponding to an optical skin depth of 274 nm.[23] In the case of the p-type sample since the p-type layer (550 nm) was twice thicker than the optical penetration, the excited region in this sample was almost restricted within the p-type layer. Low injection of photocarriers at the buried p-n junction resulted in weak acoustic generation from the corresponding depletion region. This fact was also revealed by the monotonic TA-induced damping oscillations (Fig. 3), indicating the responsible role of the acoustic pulses generated from the sample surfaces.[12]

It is worth mentioning that the shear waves generated from the surface of the p-type layer propagates into the

n-type buffer layer at a time delay of ~130 ps. With negligible interface acoustic reflection, the Brillouin oscillation before and after this traveling time thus discloses the difference in the acoustic detection sensitivity in media with different doping conditions.[24] However, no definitive difference in the shear phonon signal was found as the wave propagated through the *p*-*n* junction, as shown in Fig. 3. It indicates that different dopants, as well as the resultant band bending, do not modify the optoacoustic detection noticeably at the adopted laser wavelength, i.e., the photoelastic constants P_{44} are similar in the *n*-type and *p*-type media. Even with similar P_{44}, the measured oscillation phases Ψ_{TA} in two *a*-plane samples were different [Ψ_{TA} is ~30° (−100°) for the *p*-(*n*-) type sample], indicating different waveform of the shear waves initiated from different doping surfaces. Based on the observed phase difference (134° ± 37°), we then investigated the correlation between acoustic waveform and the photoinduced space charge field, which is the origin of the piezoelectric stress.

It is known that the photoinduced space charges attempt to maintain electric neutrality by compensating the built-in electric field. The built-in field thus determines the polarity and distribution of the piezoelectric stress. Previous studies indicated similar surface electricity in *a*-plane and *c*-plane GaN, and upward and downward band bending on the surfaces of *n*-type and *p*-type samples, respectively.[25,26] Due to opposite field directions, the photoinduced shear strain through the piezoelectric effect, as well as the consequent Brillouin oscillations, should have different signs. In addition, the acoustic pulsewidth could be divergent due to differences in the depletion lengths and the dominant species of drifting carriers. These effects provide further phase changes in the Brillouin oscillations in two studied *a*-plane samples, thus making the total phase difference deviate from 180°, agreeing with the experimental observations (134° ± 37°). This phase study supports our hypothesis that the shear phonon generation relies on the piezoelectric coupling and the screening of the surface fields.

Furthermore, photocarrier density also influences the strength and the distribution of the space charge field. With perturbative optical excitations, the space charge field is approximately uniform in the surface depletion region while its strength and distribution approach the conditions of the built-in electric field under strong illuminations (screening saturation).[27] Consequent acoustic amplitude saturation and the acoustic waveform variation are thus expected to arise when the pump fluence increases from the linear to the screening saturation regime. This phenomenon could serve as the second experimental evidence of the piezoelectric contribution.[4,17]

Figure 4 shows the power dependence of the amplitude and phase of the measured shear phonon oscillations in the *p*-type *a*-plane sample. When the pump fluence was less than 15 $\mu\mathrm{J/cm}^2$, the measured signal amplitude of shear phonon oscillations was observed to be proportional to the excitation power while it started to saturate under stronger pumping. Here a capacitance model was used to estimate the strength of the surface electric field.[4,17] We assumed that the photoexcited electrons and holes within the surface depletion region accumulate at the boundaries of the depletion region

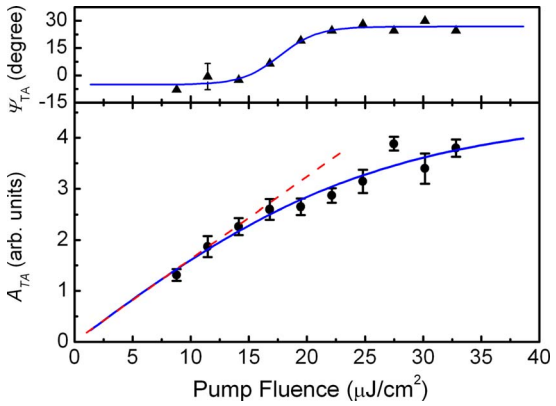

FIG. 4. (Color online) (Top) Phase Ψ_{TA} and (bottom) amplitude A_{TA} of the TA-induced Brillouin oscillations observed in the *a*-plane *p*-type sample as a function of pump fluence. Solid lines are fitting curves and the dashed line shows the linear power dependence of the oscillation amplitude in the low-excitation regime.

with two sheet distributions. The resultant space charge field under pumping with the threshold fluence P_{th} (15–20 $\mu\mathrm{J/cm}^2$) was then calculated to be ~800 kV/cm. In addition, the surface electric field can be independently evaluated using the reported surface electricity and the Schottky model, which assumes the electric field decreases linearly to zero within a depletion length L. The maximum surface electric field $E_s(z=0)$ and L are calculated from the well-known equations:[28] $E_s(z=0)=(2|e|N_A\Phi_b/\bar{\varepsilon}_S)^{1/2}$ and $L=(2\bar{\varepsilon}_S\Phi_b/|e|N_A)^{1/2}$, where N_A is the ionized doping density and Φ_b is the band bending at the surface. For *p*-type GaN, $\Phi_b \approx 1.59$ eV and $\bar{\varepsilon}_S=\varepsilon_r\varepsilon_0$, where the relative dielectric constant $\varepsilon_r=9.5$.[26] The depletion length L and the electric field $E_s(z=0)$ are thus calculated to be 58 nm and 550 kV/cm, respectively, for the studied *p*-type sample. Thus estimated surface electric fields agrees well with the observed saturation field, revealing the fact that the observed phenomenon resulted from the saturation of piezoelectric transduction in the screening saturation regime.

Accompanying with the generation saturation, a phase transition of the shear phonon signals was also observed near the threshold pump fluence, as shown in Fig. 4. It has been proved that the phase of Brillouin oscillations was related to the distribution of the propagating strain field,[29] as also found in our early observations in the samples with different surface electricity (Fig. 3). Therefore, the observed phase transition in the power-dependent examination supported our hypothesis that the change in the space charge field influenced the acoustic waveforms, which occurred when the excitation fluence was close to P_{th}.

Under intense photoexcitation ($>P_{th}$), the screening saturation of the surface electric field reduced the efficiency of the piezoelectric transduction of the shear phonons while the efficiency of the deformation transduction of longitudinal phonons remained constant. Even in the screening saturation regime, the amplitude of the shear phonon oscillations was still found to be comparable with that of the longitudinal mode (driven by the deformation potentials), as shown by data in Fig. 2. It can thus be expected that in the low-excitation regime, the piezoelectric effect can excite more

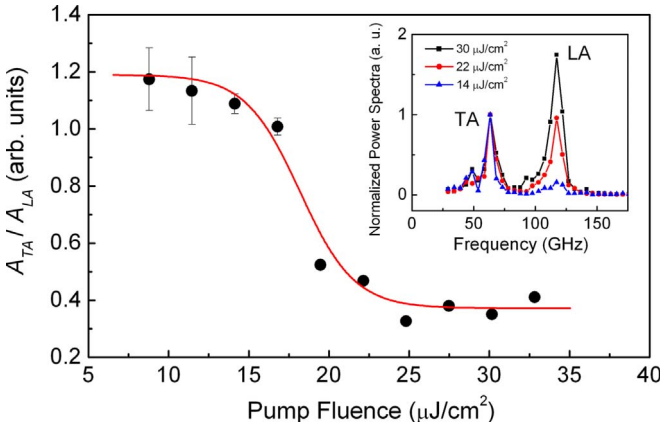

FIG. 5. (Color online) Measured ratio of the initial optical modulation intensity induced by two modes $A_{\mathrm{TA}}/A_{\mathrm{LA}}$ (dots) and the corresponding fitting curve (solid line) as a function of excitation fluence. The inset shows the Fourier power spectra of the phonon-induced transient reflectivity with different pump fluence, which were normalized by the peaks of the TA-phonon signals for clarifying the signal contrast. All data were measured in the *a*-plane *p*-type sample.

manifest coherent shear phonons in comparison with the LA phonons.

The inset of Fig. 5 shows the Fourier power spectra of the measured transient reflectivities in the *a*-plane *p*-type sample under different pump power, which were normalized according to the peak of the shear phonon component. When reducing the excitation fluence to be less than P_{th}, the strength of the LA phonons was observed to weaken rapidly in comparison with the shear phonons. The contrast enhancement of the shear mode was thus achieved as the optical excitation was in the linear regime for the piezoelectric transduction, where the spectral peak of the optically detected TA-phonon component can be found to be one order of magnitude higher than that of the LA phonon component. Figure 5 shows the corresponding ratio of the initial optical modulation intensity induced by two modes $A_{\mathrm{TA}}/A_{\mathrm{LA}}$ as a function of pump fluence. It can also be noticed that $A_{\mathrm{TA}}/A_{\mathrm{LA}}$ decreases from 1.2 to 0.4 as the excitation fluence becomes higher than P_{th}, indicating that the field saturation results in a three times reduction in the piezoelectric diving forces.

To understand the origins of the observed shear phonon signal in the linear regime, roles of the relative generation efficiency and the optical detection sensitivity for different acoustic modes should be investigated. Here we considered the Schottky model and that the studied *a*-plane *p*-type GaN was illuminated with the threshold pump fluence. The average shear stress induced by the piezoelectricity in the surface depletion region can be calculated to be $-0.5\times\bar{e}_{\mathrm{TA}}E_s(z=0)\approx 8.3$ MPa. Moreover, the initial sheet density of the photocarriers within the depletion region is $\rho_s\xi[1-\exp(-L/\xi)]$, where ρ_s is the carrier density at the surface ($\sim 8\times 10^{17}$ cm^{-3}) and ξ is the optical skin depth. At the first ~ 10 ps where the carrier diffusion outside the depletion region is not noticeable,[27] the average longitudinal stress induced by the deformation potentials in the depletion region can be formulated as $\rho_s\xi[1-\exp(-L/\xi)](\bar{d}_{e,\mathrm{LA}}+\bar{d}_{h,\mathrm{LA}})/L\approx -0.7$ MPa, where $\bar{d}_{e,\mathrm{LA}}=-4.08$ eV and $\bar{d}_{h,\mathrm{LA}}=-2.1$ eV.[13] It is noted that the calculated shear stress is 12 times higher than the longitudinal stress, corresponding to a strain ratio η_4/η_3 of ~ 44. With the measured $A_{\mathrm{TA}}/A_{\mathrm{LA}}\sim 1.2$, the optical detection sensitivity of LA phonons can be estimated to be higher than that of TA phonons by ~ 35 times. Low detection sensitivity of TA phonons has been a well-known problem, which was recently improved by using transient polarimetry.[11] Here, the contrast of the shear phonon signal was independently enhanced by controlling anisotropic piezoelectric transduction [$\bar{e}_{\mathrm{LA}}=0.73(0)$ C/m^2, $\bar{e}_{\mathrm{TA}}=0(-0.3)$ C/m^2, at $\theta=0°$ (90°)], which simultaneously improved/reduced the excitation of shear/longitudinal mode as θ changed from 0° to 90°.

In summary, we studied the piezoelectric generation of coherent shear phonons in orientated wurtzite semiconductors. By manipulating anisotropic piezoelectric stress in samples with different surface cuts, the optical modulation intensity induced by coherent shear phonons can be higher than that by LA phonons. The relevant role of the piezoelectric coupling was confirmed by looking into the correlation between surface electric field and the generated shear waves. Under strong illuminations, the intense screening of the surface electric field caused a saturation of the piezoelectric contribution and could also modify the waveform of the excited shear waves.

The authors would like to acknowledge G.-W. Chern, T. Pezeril, and O. Matsuda for inspiring scientific discussions and also thank P.-H. Wang for the technical supports. This work was sponsored by National Science Council of Taiwan under Grant No. NSC-98-2120-M-002-001 and MediaTek.

*Author to whom correspondence should be addressed; sun@cc.ee.ntu.edu.tw

[1] T. C. Zhu, H. J. Maris, and J. Tauc, Phys. Rev. B **44**, 4281 (1991).
[2] C.-K. Sun, J.-C. Liang, and X.-Y. Yu, Phys. Rev. Lett. **84**, 179 (2000).
[3] C. Rossignol, J. M. Rampnoux, M. Perton, B. Audoin, and S. Dilhaire, Phys. Rev. Lett. **94**, 166106 (2005).
[4] O. Matsuda, O. B. Wright, D. H. Hurley, V. E. Gusev, and K. Shimizu, Phys. Rev. Lett. **93**, 095501 (2004).
[5] T. Pezeril, P. Ruello, S. Gougeon, N. Chigarev, D. Mounier, J.-M. Breteau, P. Picart, and V. Gusev, Phys. Rev. B **75**, 174307 (2007).
[6] R. N. Kini, A. J. Kent, N. M. Stanton, and M. Henini, Appl. Phys. Lett. **88**, 134112 (2006).
[7] O. Matsuda, O. B. Wright, D. H. Hurley, V. E. Gusev, and K. Shimizu, Phys. Rev. B **77**, 224110 (2008).
[8] S. Dixon, C. Edwards, D. B. Palmer, and D. W. Schindel, J.

Phys. D **29**, 1345 (1996).
[9] B. Audoin, H. Meri, and C. Rossignol, Phys. Rev. B **74**, 214304 (2006).
[10] D. H. Hurley, O. B. Wright, O. Matsuda, V. E. Gusev, and O. V. Kolosov, Ultrasonics **38**, 470 (2000).
[11] D. Mounier, E. Morozov, P. Ruello, J.-M. Breteau, P. Picart, and V. Gusev, Eur. Phys. J. Spec. Top. **153**, 243 (2008).
[12] K.-H. Lin, C.-T. Yu, Y.-C. Wen, and C.-K. Sun, Appl. Phys. Lett. **86**, 093110 (2005).
[13] G. D. Sanders, C. J. Stanton, and C. S. Kim, Phys. Rev. B **64**, 235316 (2001). The deformation potentials only contribute to diagonal parts of the stress tensor and are approximately isotropic.
[14] O. B. Wright, B. Perrin, O. Matsuda, and V. E. Gusev, Phys. Rev. B **64**, 081202 (2001).
[15] O. Ambacher, J. Smart, J. R. Shealy, N. G. Weimann, K. Chu, M. Murphy, W. J. Schaff, L. F. Eastman, R. Dimitrov, L. Wittmer, M. Stutzmann, W. Rieger, and J. Hilsenbeck, J. Appl. Phys. **85**, 3222 (1999).
[16] D. Royer and E. Dieulesaint, *Elastic Waves in Solids* (Springer, New York, 2000).
[17] C.-T. Yu, K.-H. Lin, C.-L. Hsieh, C.-C. Pan, J.-I. Chyi, and C.-K. Sun, Appl. Phys. Lett. **87**, 093114 (2005).
[18] T.-S. Ko, T.-C. Wang, R.-C. Gao, H.-G. Chen, G.-S. Huang, T.-C. Lu, H.-C. Kuo, and S.-C. Wang, J. Cryst. Growth **300**, 308 (2007).
[19] J. F. Nye, *Physical Properties of Crystals* (Oxford University Press, Oxford, 1957).
[20] O. Matsuda and O. B. Wright, Anal. Sci. **17**, S216 (2001).
[21] GaN is weakly birefringent and its refractive index was taken from M. Bass, *Handbook of Optics*, 2nd ed. (McGraw-Hill, New York, 1994), Vol. 2.
[22] According to Ref. 15, sound velocities of the fast and the slow TA modes are 4689 and 4092 m/s, respectively.
[23] The characteristic propagation lengths of the observed LA and TA waves are similar (the deviation is less than the fitting uncertainty of 10%), which are limited by either acoustic attenuation or optical skin depth. Because the attenuation coefficient of 117 GHz LA waves is less than 4.2×10^{4} m^{-1} (corresponding to a propagation length of $\sim$24 μm), the sub-μm optical penetration determines the damping rate of the Brillouin oscillations in the studied case.
[24] F. Hudert, A. Bartels, T. Dekorsy, and K. Kohler, J. Appl. Phys. **104**, 123509 (2008).
[25] S. Chevtchenko, X. Ni, Q. Fan, A. A. Baski, and H. Morkoc, Appl. Phys. Lett. **88**, 122104 (2006).
[26] S. Barbet, R. Aubry, M.-A. di Forte-Poisson, J.-C. Jacquet, D. Deresmes, T. Melin, and D. Theron, Appl. Phys. Lett. **93**, 212107 (2008).
[27] Y. Rosenwaks, B. R. Thacker, R. K. Ahrenkiel, A. J. Nozik, and I. Yavneh, Phys. Rev. B **50**, 1746 (1994).
[28] S. M. Sze, *Physics of Semiconductor Devices*, 2nd ed. (Wiley, New York, 1981).
[29] M. Tomoda, O. Matsuda, O. B. Wright, and R. L. Voti, Appl. Phys. Lett. **90**, 041114 (2007).